Proceedings World Geothermal Congress 2020+1
Reykjavik, Iceland, April - October 2021

Comparisons of Heat Extraction Performances for a Multilateral-well Enhanced Geothermal System with CO_2 and Water as Working Fluids

Yu Shi, Xianzhi Song*, Gaosheng Wang, Guofeng Song, Jiacheng Li

State Key Laboratory of Petroleum Resources and Prospecting, China University of Petroleum, Beijing, Beijing 102249, China

yushicupb@gmail.com, songxz@cup.edu.cn, 371179440@qq.com, 1968068343@qq.com

Keywords: geothermal energy; enhanced geothermal system; heat extraction performance; working fluid; CO_2

ABSTRACT

Increasing studies were conducted to compare heat extraction performances of CO_2-EGS and water-EGS. However, these research efforts never considered CO_2 expansion effect in wellbore, which could not provide accurate enough comparisons between CO_2-EGS and water-EGS. Hence, based on a reservoir and wellbore coupling model, this paper comprehensively compares heat extraction performances of a multilateral-well CO_2-EGS and water-EGS considering the CO_2 pressure work in wellbore. The temperature, pressure and output thermal power distributions of multilateral-well CO_2-EGS and water-EGS are analyzed. Multiple cases for multilateral-well CO_2-EGS and water-EGS are investigated, including assessment of differences in heat extraction using varying well depths and reservoir pressures. Results show that when CO_2-EGS mass flow rate is three times of water-EGS mass flow rate, the reservoir outlet thermal power of CO_2-EGS and water-EGS is similar. However, the CO_2-EGS has much lower wellhead thermal power than water-EGS, due to the noticeable temperature reduction in CO_2-EGS wellbore induced by the CO_2 expansion. Additionally, the CO_2-EGS can perform better in a geothermal reservoir with a smaller well depth and higher reservoir pressure.

1. INTRODUCTION

CO_2 and water are the most common working fluids for the EGS. The CO_2-EGS concept using supercritical CO_2 instead of water as the EGS working fluid was first proposed by Brown (2000). Many studies (Pruss 2006; Pruss 2008; Luo et al. 2014; Pan et al. 2015; Cao et al. 2016; Borgia et al. 2012) demonstrated that CO_2-EGS had several advantages, such as the large buoyancy forces, gas-like viscosity, liquid-like density, no dissolving rock minerals and partially CO_2 sequestration. Additionally, massive studies have been conducted to compare the heat extraction performances of the EGS with CO_2 and water as the working fluids. Pruess (2006, 2008) conducted a simulation analysis on a five-spot-well EGS to find that when the CO_2 mass flow rate was four times of water, CO_2 was superior to water in the ability to extract heat. He also found that the CO_2-EGS performance was significantly affected by the reservoir pressure and the production well perforation interval. Luo et al. (2014) demonstrated that when the CO_2 mass flow rate was two times of water, the reservoir outlet temperature of the water-EGS was slightly higher than that of the CO_2-EGS, and the water-EGS and CO_2-EGS had the same lifetime. Cao et al. (2016) found that under a certain pressure drop, the CO_2-EGS had the higher mass flow rate and higher heat extraction rate than the water-EGS, but the lifetime of the CO_2-EGS was shorter.

Most of the aforementioned studies indicated that a CO_2-EGS could obtain a better heat extraction performance than a water-EGS. The conclusions in these studies were obtained mainly based on the reservoir outlet temperature from a reservoir model, which did not consider the fluid flow and heat transfer in the wellbore. However, some previous studies revealed that the CO_2 expansion had significant effects on the CO_2 temperature distribution in the wellbore. For example, Pan et al. (2015) used a reservoir and wellbore coupling model to study the heat extraction performance of a CO_2-EGS, and found that the wellhead outlet temperature of the CO_2-EGS was closely related to the pressure distribution in the wellbore. Phuoc et al. (2019) pointed out that the CO_2 expansion in the production well could induce a large heat loss and noticeably affect the CO_2 wellhead temperature. Li et al. (2017) found that the CO_2 expansion significantly affected the CO_2 wellbore temperature distribution in a wide $CO2$ flow rate range. Shi et al. (2019a) analyzed the temperature and pressure distributions of a CO_2-EGS using a reservoir and wellbore coupling model, and found that the CO_2 pressure work could lead to a dramatic temperature reduction in the production well. Therefore, using the reservoir outlet temperature rather than the wellhead outlet temperature to compare the heat extraction performances of the CO_2-EGS and water-EGS is not accurate enough. It is necessary to accurately estimate the heat extraction performances of the CO_2-EGS and water-EGS through a reservoir and wellbore coupling model considering the CO_2 expansion effect in the wellbore.

We previously proposed a multilateral-well EGS using a single main wellbore to achieve injection and production (Song et al. 2018; Shi et al.2018). The previous study (Song et al. 2018) demonstrated that the multilateral wells could enhance the injectivity and productivity of the EGS and obtain a remarkable heat extraction performance. **Figure 1** illustrates a schematic of this multilateral-well EGS process (Song et al. 2018). The previous studies (Song et al. 2018; Shi et al. 2018; Shi et al. 2019a; Shi et al. 2019b; Shi et al. 2019c) analyzed the temperature distributions of the multilateral-well EGS and investigated the effects of complex fracture networks on the heat extraction performance of the multilateral-well EGS. However, the heat extraction performances of the multilateral-well EGS with different working fluids have never yet been compared. Therefore, based on a reservoir and wellbore coupling model, this paper comprehensively compares the heat extraction performances of a multilateral-well EGS with CO_2 and water as the working fluids. The temperature, pressure and output thermal power distributions of the multilateral-well CO_2-EGS and water-EGS are compared. Multiple cases are studied for the multilateral-well CO_2-EGS and water-EGS, considering the differences in their heat extraction using varying wellbore depths, injection temperatures, mass flow rates and reservoir pressures.

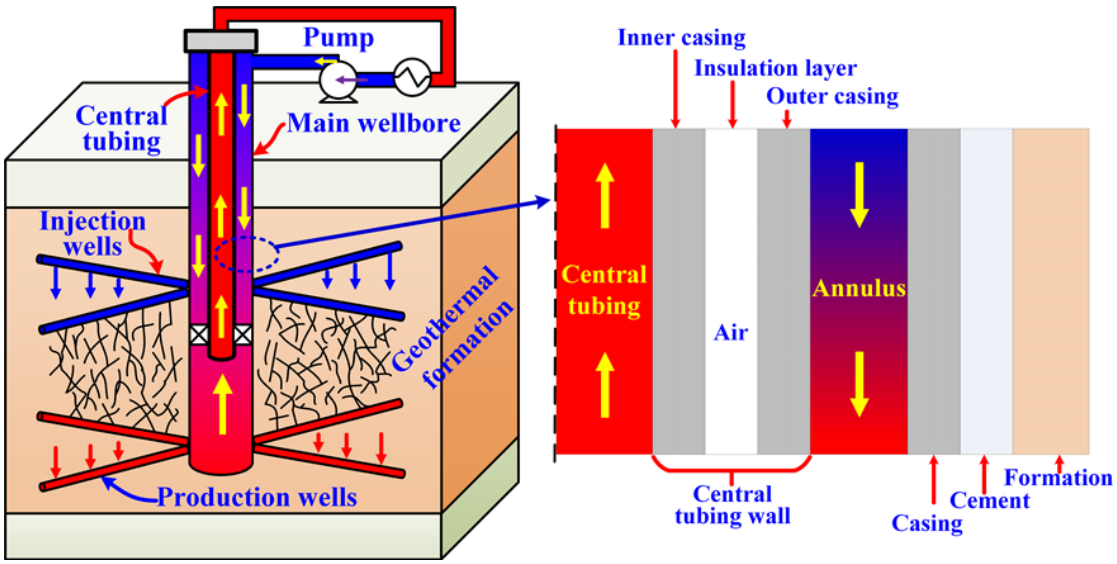

Figure 1: The schematic diagram of heat extraction for a multilateral-well EGS (Song et al. 2018) and the structure of central tubing (Shi et al. 2019a)

2. MODEL DEVELOPMENT

2.1 Thermophysical properties of the working fluids

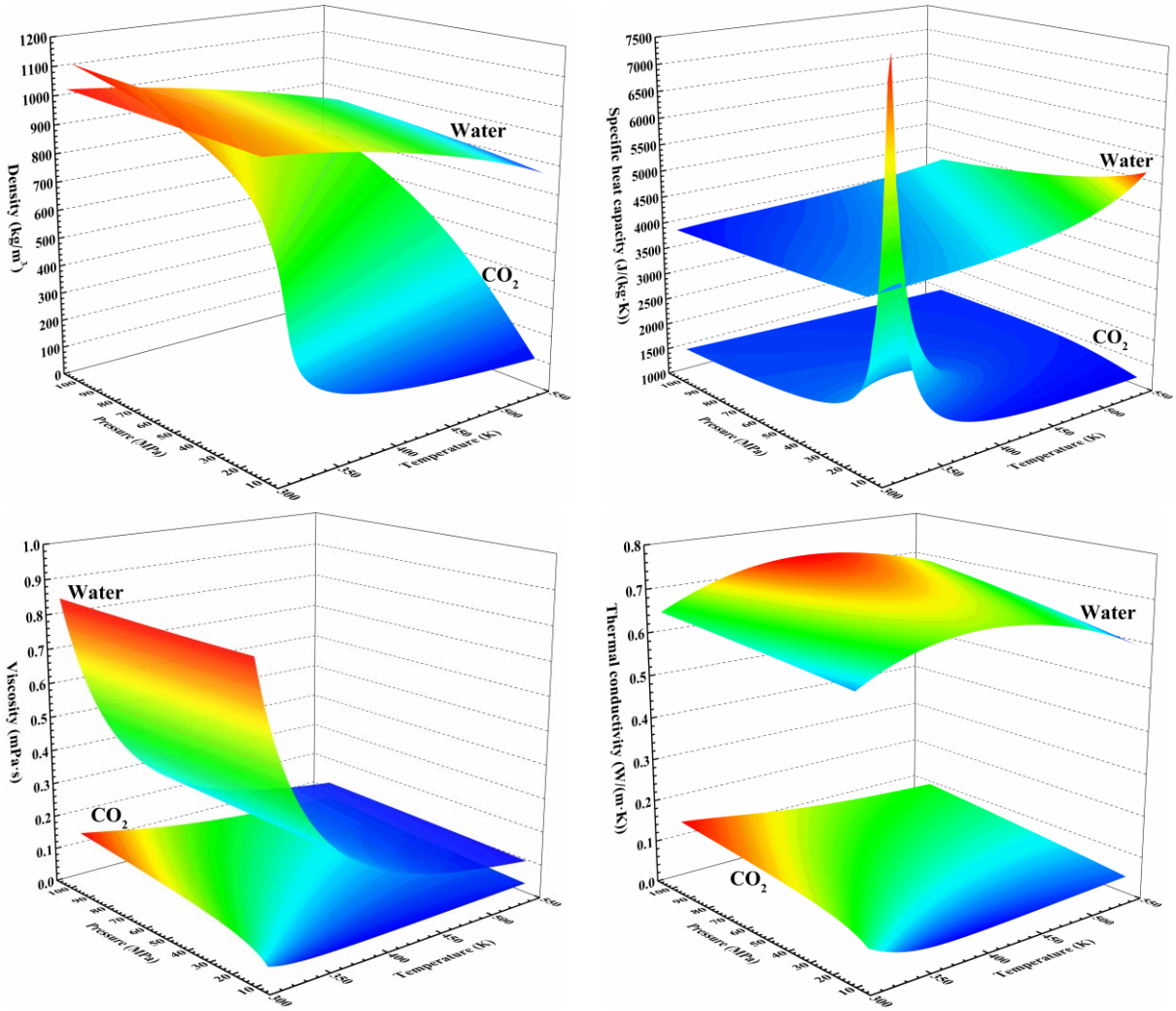

Figure 2: Comparisons of thermophysical properties for CO_2 and water (the red represents the high value and the blue indicates the low value)

In this paper, the CO_2 density and specific heat capacity are calculated by a CO_2 equation of state developed by Span and Wagner (S-W EOS) (Span and Wagner, 1996), while CO_2 viscosity and thermal conductivity are obtained from equations developed by Heidaryan et al. (Heidaryan et al. 2011) and Jarrahian et al. (Jarrahian and Heidaryan, 2012). The thermophysical properties of water are described as a function of temperature and pressure according to the NIST (National Institute of Standards and Technology) database (Linstrom and Mallard, 2001). **Figure 2** illustrates the thermophysical properties of water and CO_2 vs. the temperature and pressure. In the figure, the red represents the high value and the blue indicates the low value. Under the typical EGS conditions (423-473 K, 10-60 MPa), the properties of water including density, specific heat capacity, viscosity and thermal conductivity are much higher than those of CO_2. Particularly the specific heat capacity of water is about 2.5 to 3 times higher than that of CO_2. The temperature has more significant effects on the thermophysical properties than the pressure for water, while the CO_2 properties strongly depend on both the pressure and the temperature. Additionally, the CO_2 density varies noticeably with the temperature and pressure, and the water viscosity is obviously influenced by the temperature. Near the critical point (31.1 ºC, 7.38 MPa) of CO_2, there is a singularity for the CO_2 specific heat capacity.

2.2 Mathematical equations

Our previous study has presented a geothermal reservoir and wellbore coupling model (Song et al. 2018). The mass conservation and momentum equations in the central tubing and annulus are expressed as:

$$\frac{\partial\left(A_p\rho_f\right)}{\partial t}+\nabla\cdot\left(A_p\rho_f u\right)=0 \tag{1}$$

$$\rho_f\frac{\partial u}{\partial t}=-\nabla p-\frac{1}{2}f_D\frac{\rho_f}{d_p}|u|u-\rho_f g \tag{2}$$

where A_p (m^2) represents the cross section area of central tubing and ρ_f (kg/m^3) is the working fluid density. The symbol u (m/s) and p (Pa) are the velocity and pressure. d_p (m) and g (m/s^2) are the central tubing hydraulic diameter and gravitational acceleration. In Eq. (2), the second term on the right denotes the pressure loss in the tubing and annulus induced by the working fluid viscosity shear. The parameter f_D is the Darcy friction factor.

Eqs. (3) and (4) are used to describe the energy conservation in the central tubing and annulus.

$$\rho_f A_p c_{p,f}\frac{\partial T}{\partial t}+\rho_f A_p c_{p,f}u\cdot\nabla T=\nabla\cdot\left(A_p\lambda_f\nabla T\right)+\frac{1}{2}f_D\frac{\rho_f A_p}{d_p}|u|u^2-A_pT\alpha_p\left(\frac{\partial p}{\partial t}+u\cdot\nabla p\right)-Q_1 \tag{3}$$

$$\rho_f A_p c_{p,f}\frac{\partial T}{\partial t}+\rho_f A_p c_{p,f}u\cdot\nabla T=\nabla\cdot\left(A_p\lambda_f\nabla T\right)+\frac{1}{2}f_D\frac{\rho_f A_p}{d_p}|u|u^2-A_pT\alpha_p\left(\frac{\partial p}{\partial t}+u\cdot\nabla p\right)+Q_1+Q_2 \tag{4}$$

where $c_{p,f}$ (J/(kg·ºC)) and T (ºC) denote the working fluid heat capacity and temperature. λ_f (W/(m·ºC)) is the working fluid heat conductivity. The second term on the right of Eqs. (3) and (4) denotes the working fluid dissipated frictional heat. The third term on the right indicates the gas pressure work induced by expansion. The parameter α_p (1/ ºC) is the thermal expansion coefficient. The term Q_1 (W/m) represents the heat exchange between the central tubing and annulus, while Q_2 (W/m) represents the heat exchange between the annulus and the surrounding formation through the casing.

In the geothermal reservoir, the reservoir rock is assumed to be homogeneous and isotropic and the fluid flow is modelled by the Darcy's Law.

$$\frac{\partial\left(\varphi\rho_f\right)}{\partial t}-\nabla\cdot\left(\rho_f u\right)=0 \tag{5}$$

$$u=\frac{k}{\mu_f}\left(\nabla p+\rho_f g\nabla z\right) \tag{6}$$

where parameters φ and μ_f (Pa·s) represent the reservoir porosity and the fluid viscosity. k (m^2) is the rock matrix permeability. In this paper, the heat transfer in the geothermal reservoir is modelled by the local thermal equilibrium equation. The energy conservation equation for the reservoir is written as:

$$\left(\rho c_p\right)_{eff}\frac{\partial T}{\partial t}+\rho_f c_{p,f}u\cdot\nabla T-\nabla\cdot\left(\lambda_{eff}\nabla T\right)=0 \tag{7}$$

where $(\rho c_p)_{eff}$ and λ_{eff} are the effective volumetric capacity and the effective thermal conductivity.

3. INITIAL AND BOUNDARY CONDITIONS

The mathematical equations are solved in the finite element solver COMSOL. The computational model including a 1D wellbore and a 3D geothermal reservoir, which can be found in the reference (Shi et al. 2019a). The previous study (Shi et al. 2019a) also

demonstrated the detailed explanations on the coupling process of the 3D reservoir model and 1D wellbore model. The parameters input in the model are listed in **Table 1**.

Table 1: Properties of the geothermal reservoir

Items	Density (kg/m^3)	Heat conductivity (W/(m·ºC))	Heat capacity (J/(kg·ºC))	Porosity	Permeability (m^2)
Enclosing rock	2800	3	1000	1	10^{-18}
SRV	2700	2.8	1000	15	2×10^{-15}

For the 1D wellbore model, the initial temperatures in the central tubing and annulus are 40 ºC. The annulus wellhead temperature remains constant at 40 ºC. The annulus wellhead mass flow rates of the CO_2-EGS and water-EGS are fixed at 80 kg/s and 25 kg/s, respectively. The annulus bottomhole pressure is equal to the average pressure of the injection lateral wells obtained from the 3D reservoir model. The central tubing bottomhole temperature and pressure are equal to the average temperature and pressure of the production lateral wells calculated from the 3D reservoir model. The mass flow rates at the central tubing outlet for the CO_2-EGS and water-EGS remain constant at 80 kg/s and 25 kg/s. For the formation around the 1D wellbore, the temperature gradient is 0.05 ºC/m with a ground temperature of 30 ºC. For the 3D reservoir model, the initial temperature and pressure increase linearly from the top to the bottom boundary. The temperature and pressure at the top boundary are 190 ºC and 30 MPa. The geothermal and pressure gradients are 0.05 ºC /m and 10000 Pa/m. The top boundary is considered to be insulated due to a cap rock above the reservoir. The temperatures on the bottom and side boundaries remain constant at the initial reservoir temperature. A no-flow condition is imposed at all boundaries. The temperature of the injection lateral wells is equal to the annulus bottomhole temperature calculated from the 1D wellbore. The injection lateral wells mass flow rates of the CO_2-EGS and water-EGS are 80 kg/s and 25 kg/s.

4. RESULTS AND DISCUSSIONS

4.1 Comparisons of multilateral-well CO_2-EGS and water-EGS

Generally, the specific heat capacity of water is about 2.5 to 3 times higher than CO_2 specific heat capacity (**Figure 2**). Therefore, to extract the same amount of heat, the mass flow rate of CO_2 should be about 3 times larger than water mass flow rate. The mass flow rates of the CO_2-EGS and water-EGS are set as 80 kg/s and 25 kg/s, respectively. **Figure 3** shows the 30-year temperatures at the bottomhole and wellhead of the central tubing and annulus for the multilateral-well CO_2-EGS and water-EGS. At the central tubing bottomhole (or at the production lateral wells), the production temperature of the multilateral-well CO_2-EGS is the same as the water-EGS production temperature before 21-years production. After 21 years, the CO_2-EGS temperature decreases rapidly due to the thermal breakthrough, while the thermal breakthrough is not observed during the entire 30-years production for the water-EGS. The central tubing wellhead temperature of the water-EGS approximates to the central tubing bottomhole temperature and is much higher than the central tubing wellhead temperature of the CO_2-EGS. At the annulus bottomhole (or at the injection lateral wells), the injection temperature of the CO_2-EGS is about 17 ºC higher than the water-EGS injection temperature.

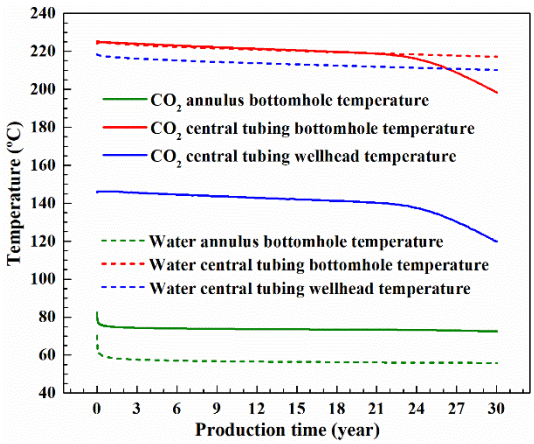

Figure 3: 30-year temperatures at wellhead and bottomhole of central tubing and annulus for multilateral-well CO_2-EGS and water-EGS

Figure 4 illustrates annulus and central tubing temperature distributions along the well depth after 30-years production of the multilateral-well CO_2-EGS and water-EGS. It can be observed that under the same injection temperature at annulus wellhead, the CO_2-EGS annulus temperature is increasingly higher than the water-EGS annulus temperature along the well depth. Additionally, there is a noticeable temperature reduction (over 70 ºC) from the central tubing bottomhole to wellhead for the CO_2-EGS, while the temperature in the central tubing of the water-EGS just decreases slightly, less than 8 ºC. This is because the pressure work plays a key role in the wellbore heat transfer of the CO_2-EGS due to the large CO_2 compressibility. For the injection process in the annulus, the pressure gradient is positive from the wellhead to bottomhole, so the pressure work contributes to the higher temperature of CO_2-EGS than water-EGS. For the production process in the central tubing, the pressure gradient is negative from the bottomhole to wellhead, so the pressure work causes a dramatic temperature reduction of the CO_2-EGS.

Figure 5 shows the 30-year pressures at the wellhead and bottomhole of the central tubing and annulus for the multilateral-well CO_2-EGS and water-EGS. In the geothermal reservoir, the injection pressure at injection lateral wells (annulus bottomhole pressure) of the water-EGS is larger than that of the CO_2-EGS, while the production pressure at production lateral wells (central tubing bottomhole pressure) of the water-EGS is lower than that of the CO_2-EGS. Therefore, though the mass rate of CO_2 is over 3 times larger than

water mass rate, the pressure loss consumed in the geothermal reservoir for the water-EGS is still higher than the CO_2-EGS. This can be also found from **Figure 6**, which plots 30-year pressure losses in the geothermal reservoir, annulus and central tubing of the CO_2-EGS and water-EGS. The pressure losses in the geothermal reservoir of CO_2-EGS and water-EGS are about 16 MPa and 26 MPa, respectively. This indicates that CO_2 has lower flow resistance in the reservoir than water, due to the much lower viscosity of CO_2 than water viscosity (**Figure 2**). Additionally, the pressure loss in the central tubing of the CO_2-EGS is noticeably high, while the pressure losses in central tubing and annulus of the water-EGS are negligible. This is because the much higher velocity of CO_2 in the central tubing causes a much larger frictional pressure drop than water. Also, it can be observed from **Figure 5** that the pressure difference between annulus wellhead and central tubing wellhead for the CO_2-EGS is 15 MPa, much lower than the pressure difference (about 22 MPa) for water-EGS. This indicates that the density difference of CO_2 induces buoyancy forces in the CO_2-EGS wellbore.

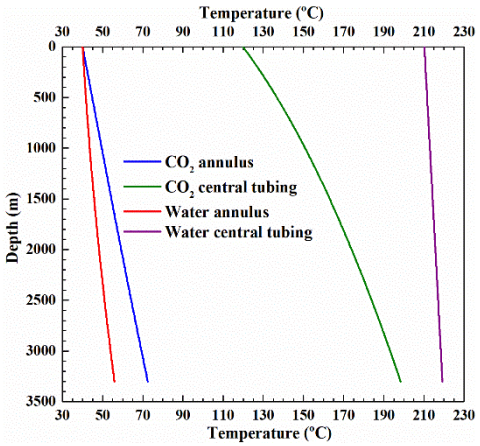

Figure 4: Annulus and central tubing temperature distributions along the depth over 30-years production of multilateral-well CO_2-EGS and water-EGS

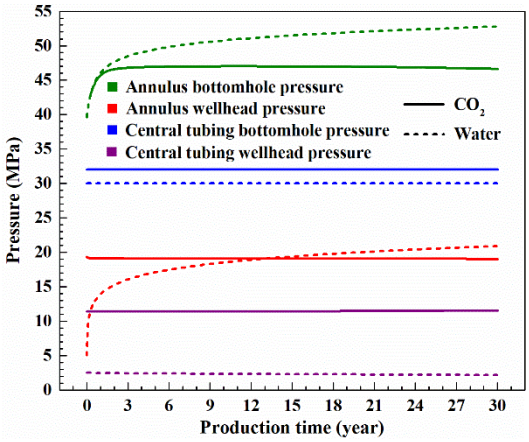

Figure 5: 30-year pressures at wellhead and bottomhole of central tubing and annulus for multilateral-well CO_2-EGS and water-EGS

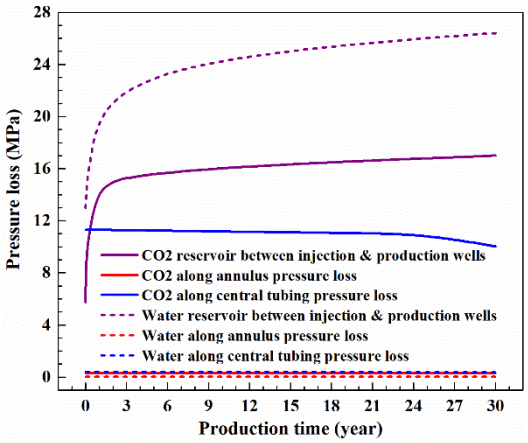

Figure 6: 30-year pressure losses in the geothermal reservoir, annulus and central tubing of CO_2-EGS and water-EGS

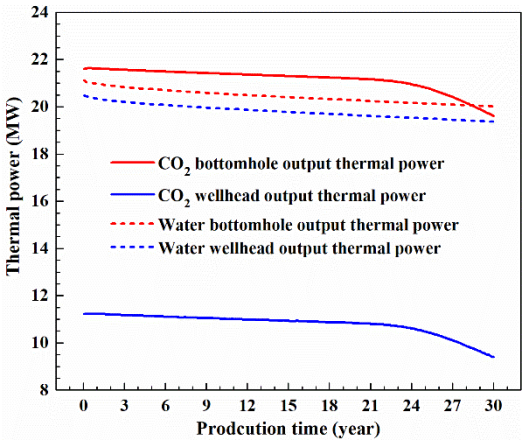

Figure 7: 30-year output thermal power at bottomhole and wellhead of central tubing for multilateral-well CO_2-EGS and water-EGS

Figure 7 compares the output thermal power at the bottomhole and wellhead of central tubing for the multilateral-well CO_2-EGS and water-EGS. At the bottomhole of central tubing, the output thermal power of CO_2-EGS and water-EGS is indeed similar and the output thermal power of the CO_2-EGS is even slightly higher than that of the water-EGS. However, at the later production stage, the output thermal power of the CO_2-EGS is lower than the water-EGS output thermal power due to the thermal breakthrough occurring in the CO_2-EGS. Furthermore, the central tubing wellhead output thermal power of the water-EGS is above 20 MW, slightly lower than the bottomhole output thermal power. The output thermal power at the central tubing wellhead of the CO_2-EGS is about 11 MW before 24-years production, 10 MW lower than bottomhole output thermal power, which is caused by the significant temperature drawdown in the central tubing.

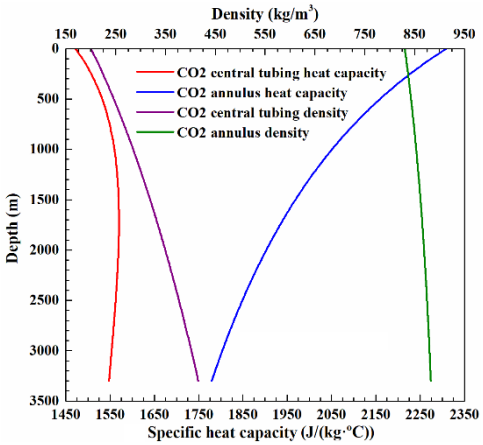

Figure 8: Annulus and central tubing CO_2 density and heat capacity distributions along the well length after 30 years

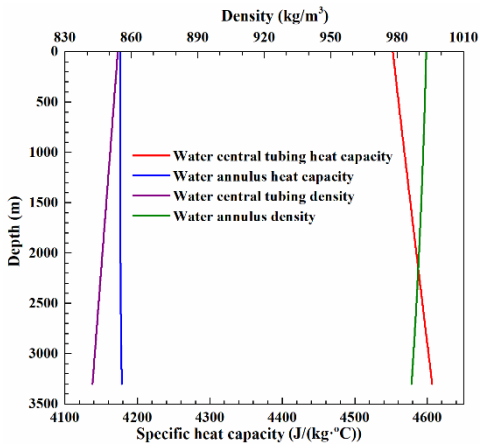

Figure 9: Annulus and central tubing water density and heat capacity distributions along the well length after 30 years

The annulus and central tubing density and heat capacity distributions along the well depth after 30-years production for multilateral-well CO_2-EGS and water-EGS are illustrated in **Figures 9** and **10**. In the CO_2-EGS, the density and specific heat capacity of CO_2 vary significantly along the well depth, while the water properties of the water-EGS show minor changes in the annulus and central

tubing. For example, the density and specific heat capacity of CO_2 vary from 175 kg/m^3 to 880 kg/m^3 and 1340 J/(kg·ºC) to 2305 J/(kg·ºC), while the water density and specific heat capacity just change from 842 kg/m^3 to 993 kg/m^3 and 4178 J/(kg·ºC) to 4606 J/(kg·ºC). This indicates that CO_2 properties are highly sensitive to pressure and temperature and water-EGS has a more stable heat extraction than CO_2-EGS.

Through above comparisons between the CO_2-EGS and water-EGS, we can conclude that when the mass flow rate of CO_2 is about 3 times of the water mass flow rate, the bottomhole output thermal power of the multilateral-well CO_2-EGS and water-EGS is similar. Due to the higher flow rate of CO_2, the CO_2-EGS shows earlier thermal breakthrough than the water-EGS. However, CO_2 has a large compressibility, so the pressure work plays a key role in the wellbore heat transfer of the CO_2-EGS. The pressure work induces a higher annulus temperature of the CO_2-EGS than the water-EGS and a noticeable temperature reduction in the central tubing of the CO_2-EGS. Therefore, at the wellhead of central tubing, the production temperature and output thermal power of the CO_2-EGS are much lower than those of the water-EGS. The large CO_2 density difference between the central tubing and annulus provides the buoyancy force for the CO_2-EGS, so the pressure difference between annulus wellhead and central tubing wellhead of the CO_2-EGS is lower than the water-EGS. Though the buoyancy effect may compensate for the energy required for the CO_2 circulation, the central tubing dramatic temperature reduction makes the output thermal power of the multilateral-well CO_2-EGS much less than water-EGS. Therefore, a multilateral-well water-EGS has a more stable operational process and better heat extraction performance than a multilateral-well CO_2-EGS.

4.2 Effect of well depth

Figures 10 and **11** illustrate 30-years central tubing well head temperatures and output thermal power for the multilateral-well CO_2-EGS and water-EGS under various well depths. The well depth indicates the depth where the injection lateral wells are located. As the well depth decreases, the central tubing wellhead temperature and output thermal power of the CO_2-EGS noticeably increase. For example, when the well depth decreases from 3300 m to 2000 m, the central tubing wellhead temperature and output thermal power of the CO_2-EGS improve 38 ºC and 5 MW. This is because the decreasing of the well depth reduces the CO_2 pressure work. However, the central tubing well head temperature and thermal power of the water-EGS just rises slightly with the decrease of well depth, due to the less heat exchange between the central tubing and annulus. Therefore, this suggests that the CO_2-EGS is more appropriate for a shallow geothermal reservoir than for a deep geothermal reservoir. The well depth has a negligible effect on the heat extraction performance of the water-EGS.

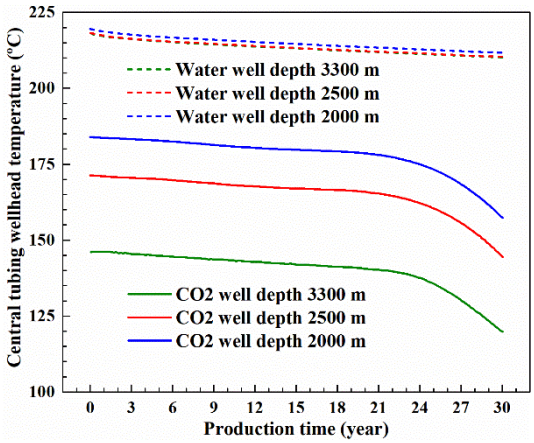

Figure 10: 30-years central tubing wellhead temperatures for multilateral-well CO_2-EGS and water-EGS under various well depths

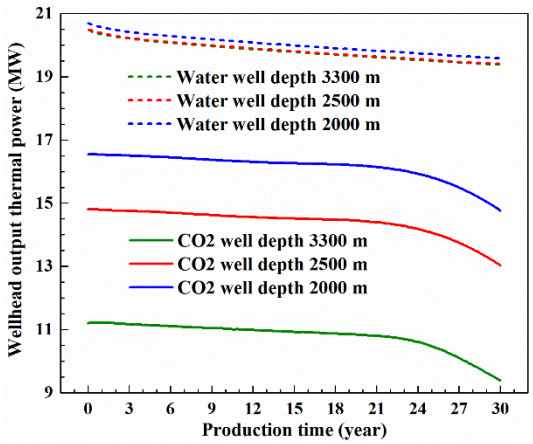

Figure 11: 30-years central tubing wellhead output thermal power for multilateral-well CO_2-EGS and water-EGS under various well depths

4.3 Effect of reservoir pressure

Figures 12 and **13** plot the 30-years central tubing wellhead temperatures and production pressure differences for the multilateral-well CO_2-EGS and water-EGS under various reservoir pressures. The reservoir top pressure mentioned in the figures indicates the pressure on the top boundary of the reservoir computational model. As the reservoir pressure increases, the central tubing well head temperature of the CO_2-EGS improves dramatically. For example, when the reservoir pressure rises from 40 MPa to 60 MPa, the CO_2-EGS central tubing wellhead temperature increases by 20 ºC. Under the higher pressure, the CO_2 expansivity in the central tubing decreases, which reduces the CO_2 pressure work. Therefore, the CO_2 temperature reduction in the central tubing induced by the pressure work is weakened under the higher pressure. Additionally, the production pressure difference of the CO_2-EGS only rises a little with the increase of reservoir pressure. Hence, we can conclude that a higher reservoir pressure is beneficial for the heat extraction performance of the multilateral-well CO_2-EGS. Also, we can from **Figures 12** and **13** that dash lines for the water-EGS under various reservoir pressures are overlapped. This means that the reservoir pressure has no effects on the central tubing wellhead temperature and production pressure difference of the water-EGS.

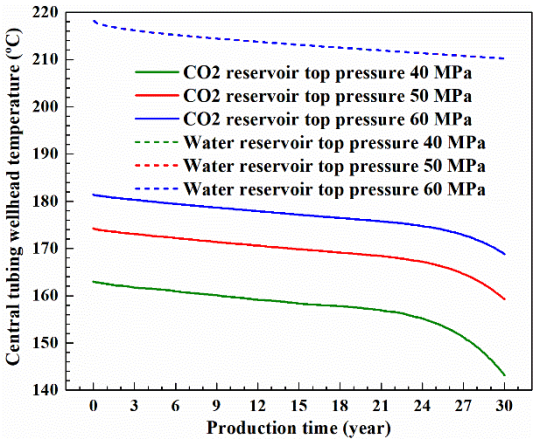

Figure 12: 30-years central tubing wellhead temperatures for multilateral-well CO_2-EGS and water-EGS under various reservoir pressures (dash lines for water-EGS are overlapped)

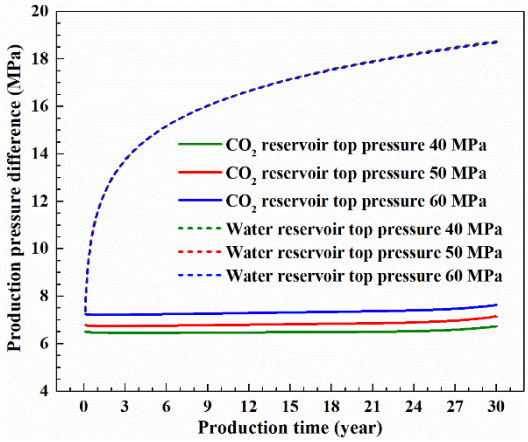

Figure 13: 30-years production pressure differences for multilateral-well CO_2-EGS and water-EGS under various reservoir pressures (dash lines for water-EGS are overlapped)

5. CONCLUSIONS

In this paper, the heat extraction performances of the multilateral-well CO_2-EGS and water-EGS are compared based on a reservoir and wellbore coupling model considering the CO_2 expansion effect in the wellbore. The temperature distribution, pressure distribution and output thermal power of the multilateral-well CO_2-EGS and water-EGS are analyzed. The effects of well depth on the multilateral-well CO_2-EGS and water-EGS performances are evaluated. The differences in heat extraction of the multilateral-well CO_2-EGS and water-EGS using varying reservoir pressures are studied. Based on the setup of the computational model and assumptions made in this paper, the key findings are as follows:

•When the mass flow rate of CO_2 is about 3 times of water mass flow rate, the bottomhole output thermal power of the multilateral-well CO_2-EGS and water-EGS is similar. However, the CO_2-EGS shows earlier thermal breakthrough than the water-EGS Due to the higher flow rate of CO_2. The CO_2 pressure work makes the CO_2-EGS annulus temperature higher than the water-EGS and induces a noticeable temperature reduction in the central tubing of the CO_2-EGS. Therefore, at the wellhead of central tubing, the production temperature and output thermal power of the CO_2-EGS are much lower than those of the water-EGS. The large CO_2 density difference between the central tubing and annulus provides the buoyancy force for the CO_2-EGS, so the pressure difference between annulus wellhead and central tubing wellhead of the CO_2-EGS is lower than the water-EGS. Generally, the multilateral-well water-EGS has a more stable operational process and better heat extraction performance than the multilateral-well CO_2-EGS.

•The smaller well depth can reduce the CO_2 pressure work in the central tubing, therefore noticeably improving the central tubing wellhead temperature and output thermal power of the multilateral-well CO_2-EGS. The well depth has minimal effects on the heat extraction performance of the multilateral-well water-EGS. Therefore, the multilateral-well CO_2-EGS is more appropriate for a shallow geothermal reservoir than for a deep geothermal reservoir.

•A higher reservoir pressure is able to reduce the CO_2 pressure work in the central tubing of the multilateral-well CO_2-EGS and noticeably improve the central tubing wellhead temperature. Therefore, the multilateral-well CO_2-EGS is appropriate for the geothermal reservoir with the higher pressure. However, the reservoir pressure has negligible effects on the heat extraction of the multilateral-well water-EGS.

ACKNOWLEDGEMENTS

The authors would like to acknowledge the National Key Research and Development Program of China (Grant No. 2018YFB1501804 and 2016YFE0124600) and National Natural Science Funds for Excellent Young Scholars of China (Grant No. 51822406).

REFERENCES

Borgia, A., Pruess, K., Kneafsey, T.J., Oldenburg, C.M., and Pan, L.: Numerical simulation of salt precipitation in the fractures of a CO_2-enhanced geothermal system, *Geothermics*, 44, (2012), 13-22.

Brown, D.W.: A hot dry rock geothermal energy concept utilizing supercritical CO_2 instead of water, *Proceedings,* 25th Workshop on Geothermal Reservoir Engineering, Stanford University, Stanford, CA (2000).

Cao, W., Huang, W., and Jiang, F.: Numerical study on variable thermophysical properties of heat transfer fluid affecting EGS heat extraction, *International journal of heat and mass transfer*, 92, (2016), 1205-1217.

Heidaryan, E., Hatami, T., Rahimi, M., and Moghadasi, J.: Viscosity of pure carbon dioxide at supercritical region: Measurement and correlation approach, *The Journal of Supercritical Fluids*, 56, (2011), 144-151.

Jarrahian, A., and Heidaryan, E.: A novel correlation approach to estimate thermal conductivity of pure carbon dioxide in the supercritical region, *The Journal of Supercritical Fluids,* 64, (2012), 39-45.

Linstrom, P.J., and Mallard, W.G.: The NIST Chemistry WebBook: A chemical data resource on the internet, *Journal of Chemical & Engineering Data*, 46, (2001), 1059-1063.

Li, X.J., Li, G.S., Wang, H.Z., Tian, S.C., Song, X.Z., Lu, P.Q., and Wang, M.: A unified model for wellbore flow and heat transfer in pure CO_2 injection for geological sequestration, EOR and fracturing operations, *International Journal of Greenhouse Gas Control*, 57, (2017), 102-115.

Luo, F., Xu, R.N., and Jiang, P.X.: Numerical investigation of fluid flow and heat transfer in a doublet enhanced geothermal system with CO2 as the working fluid (CO_2–EGS), *Energy*, 64, (2014), 307-322.

Pan, L., Freifeld, B., Doughty, C., Zakem, S., Sheu, M., Cutright, B., and Terrall, T.: Fully coupled wellbore-reservoir modeling of geothermal heat extraction using CO 2 as the working fluid, *Geothermics*, 53, (2015), 100-113.

Phuoc, T.X., Massoudi, M., Wang, P., and McKoy, M.L.: Heat losses associated with the upward flow of air, water, CO_2 in geothermal production wells, *International journal of heat and mass transfer*, 132, (2019), 249-258.

Pruess, K.: Enhanced geothermal systems (EGS) using CO_2 as working fluid—A novel approach for generating renewable energy with simultaneous sequestration of carbon, *Geothermics*, 35, (2006), 351-367.

Pruess, K.: On production behavior of enhanced geothermal systems with CO_2 as working fluid, *Energy Conversion and Management*, 49, (2008), 1446-1454.

Shi, Y., Song, X.Z., Li, J.C., Wang, G.S., Zheng, R. and YuLong, F.: Numerical investigation on heat extraction performance of a multilateral-well enhanced geothermal system with a discrete fracture network, *Fuel*, 244, (2019b), 207-226.

Shi, Y., Song, X.Z., Shen, Z.H., Wang, G.S., Li, X.J., Zheng, R., Geng, L.D., Li, J.C., and Zhang, S.K.: Numerical investigation on heat extraction performance of a CO_2 enhanced geothermal system with multilateral wells, *Energy*, 163, (2018), 38-51.

Shi, Y., Song, X.Z., Wang, G.S., Li, J.C. Li, X.J., and Geng, L.D.: Numerical Study on Heat Extraction performance of a Multilateral-well Enhanced Geothermal System Considering Complex Hydraulic and Natural Fractures, *Renewable Energy*, 141, (2019c), 950-63.

Shi, Y., Song, X.Z., Wang, G.S., McLennan, J., Forbes, B., Li, X.J., and Li, J.C.: Study on wellbore fluid flow and heat transfer of a multilateral-well CO_2 enhanced geothermal system, *Applied Energy*, 249, (2019a), 14-27.

Song, X.Z., Shi, Y., Li, G.S., Yang, R.Y., Wang, G.S., Zheng, R., Li, J.C., and Lyu Z.H.: Numerical simulation of heat extraction performance in enhanced geothermal system with multilateral wells, *Applied Energy*, 218, (2018), 325-337.

Span, R., and Wagner, W.: A new equation of state for carbon dioxide covering the fluid region from the triple‐point temperature to 1100 K at pressures up to 800 MPa, *Journal of physical and chemical reference data*, 25, (1996), 1509-1596.